Urokinase Exerts Antimetastatic Effects by Dissociating Clusters of Circulating Tumor Cells

Jin Woo Choi[1,2,3], Jun Ki Kim[4], Yun Jung Yang[1], Pilhan Kim[5], Kwon-Ha Yoon[2,6], and Seok Hyun Yun[7]

Abstract

Clusters of circulating tumor cells (CTC) exhibit more robust metastatic properties than single CTC. Thus, understanding the distinct behaviors of CTC clusters and how CTC clustering is regulated may offer new insights into how to limit metastasis. In this study, we utilized an *in vivo* confocal system to observe the clustering behavior of CTC in real time, finding that the number of clusters increased proportionally with the growth of the primary tumor. Our experiments also indicated that the flow rate of the CTC clusters in blood vessels was relatively slower than single CTC due to increased vessel wall adhesion. Depending on disease stage, 5% to 10% of total CTC in circulation were in clusters, with this proportion increasing to >24% within lung metastases examined. Notably, in the 4T1 mouse model of breast cancer metastasis, we found that injecting host animals with urokinase-type plasminogen activator, a clinical thrombolytic agent, was effective at preventing the assembly of CTC clusters and prolonging overall host survival by approximately 20% relative to control animals. Our results suggest a tractable approach to limit metastasis by suppressing the formation or stability of CTC clusters circulating in the blood of cancer patients. *Cancer Res; 75(21); 4474–82. ©2015 AACR.*

Introduction

In primary tumors, the capacity of the majority of cells means that they cannot metastasize into other organs. Only a limited number of primary tumor cells become the circulating tumor cells (CTC) that subsequently invade a patient's blood vessels, leading to the ultimate dissemination of such cells into the secondary organs. An increase of the number of CTCs generally means a greater likelihood of a poor survival outcome. For this reason, CTC detection has emerged as a useful practice to predict the emergence of cancer metastases and describe the progression of

the disease (1–3). Interestingly, the presence of CTC clusters as well as single CTCs in the bloodstream has been frequently reported, while it has been confirmed that CTCs form clusters in circulatory areas (4), and particularly around primary tumors (5).

The number of CTC clusters is associated with clinically important factors such as the release of cancer cells from primary tumors and the response to chemotherapy. In addition, in previous studies in which an animal model with Lewis carcinoma and melanoma cells was used, tumor-cell aggregates disproportionately generated more lung colonies than equivalent numbers of single cells after tail-vein injections (6, 7), and the yield of spontaneous metastases was influenced by the release of clumps from fibrosarcomas (7). It is therefore of great interest that the release of cancer clumps is a parameter that is quantitatively related to the overall prognosis of spontaneous metastases.

Molnar and colleagues isolated CTC clusters by using magnetic labeling and suggested that a significant correlation exists between the number of clusters and the survival outcome of patients with colon cancer (4). Studies that used metastatic cancer cell lines revealed that many CTCs exist as clumps in blood vessels, and although the number of clumps varied widely between individuals, it seemed to be highly correlated to the extent of lung colonization (8). Furthermore, the research demonstrated that the number of CTC clusters in the circulatory system can directly predict the degree of disease progression for breast cancer.

Recently, a variety of methods and devices have been developed to detect CTCs (9, 10); for example, microfluidic assay is an effective way to count and sort those CTCs in the peripheral blood (11), while the immunomagnetic cell-separation technique can also be applied to isolate cells of a specific lineage from a variety of other immune-cell types in the blood (12). Aceto and colleagues utilized new technology platforms such as the

[1]Wonkwang Institute of Integrative Biomedical Science and Dental Research Institute, School of Dentistry, Wonkwang University, Iksan, Chonbuk, Korea. [2]Imaging Science-Based Lung and Bone Diseases Research Center, Wonkwang University, Iksan, Cheonbuk, Korea. [3]Advanced Institute of Convergence Technology, Seoul National University, Suwon, Gyenggi-do, Korea. [4]Biomedical Engineering Center, Asan Institute for Life Sciences, Asan Medical Center and University of Ulsan, College of Medicine, Seoul, Korea. [5]Graduate School of Nanoscience and Technology, Korea Advanced Institute of Science and Technology, Daejeon, Korea. [6]Department of Radiology, Wonkwang University School of Medicine, Iksan, Jeonbuk, Korea. [7]Wellman Center for Photomedicine, Massachusetts General Hospital, Harvard Medical School, Boston, Massachusetts.

Note: Supplementary data for this article are available at Cancer Research Online (http://cancerres.aacrjournals.org/).

Corresponding Authors: Jin Woo Choi, Wonkwang University, Iksandaero, Iksan, Cheonbuk, 570-711, Korea. Phone: 821040473070; Fax: 8228318042; E-mail: jinwoochoi@wku.ac.kr; Kwon-Ha Yoon, Wonkwang University, Iksandaero, Iksan, Cheonbuk, 570-711, Korea. E-mail: khy1646@wku.ac.kr; and Seok Hyun Yun, Harvard Medical School, Boston, MA. E-mail: syun@hms.harvard.edu

AACR

Herringbone HBCTC-Chip and [neg]CTC-iChip to isolate and observe individual CTCs and CTC clusters (13, 14). They revealed that CTC clusters originate from oligoclonal aggregates, which are released from primary tumor cells and are more metastatic than equivalent numbers of single CTCs. Although CTC clusters are rare, their significance means that the cells they are composed of must be managed carefully during cancer treatment. However, even though these studies revealed the importance of CTCs and CTC clusters, the corresponding experiments provided only cross-sectional information on their behavior and properties without detailing the corresponding spatiotemporal dynamics. For example, important questions about the associative dynamics of CTCs that underpin cluster formation or the dissociation of CTCs from such clusters remained largely unresolved. On the basis of the real-time behavior of CTCs and CTC clusters in blood vessels, we believe that the methods for *ex vivo*–prepared samples may have an internal limitation regarding the dissection of CTCs and CTC clusters.

As CTC clusters, which coexist with single CTCs in the bloodstream of cancer patients, represent a more critical prognostic or predictive factor of the metastatic process than single circulating cells (5), a better understanding of CTC cluster formation is urgently required to treat cancer and protect against metastasis. Live-imaging–based experiments are considered the most robust method for addressing this problem (15, 16). The use of fluorescent proteins and other developments in optical-imaging technology have made it possible to directly observe cancer cells as they spread from their original site (17). To track the motility of fluorescently labeled target cells, confocal systems that operate on a millisecond time scale are particularly useful (18, 19). In this study, we used intravital, confocal fluorescence microscopy to describe the hidden behaviors of CTC clusters in comparison with those of single CTCs. By analyzing the characteristics of CTC clusters, we confirmed a hypothesis about the crucial involvement of CTC clusters in metastasis; furthermore, we investigated the inhibitory effect of urokinase on fibrin in the CTC clusters, thereby uncovering potential pharmacologic routes for the suppression of CTC clustering.

Materials and Methods

Cell and chemical preparation
Murine mammalian carcinoma cell lines 4T1, B16, and B16F10 were purchased from Korea Cell Bank. The cells were cultured in a RPMI-1649 medium (Hyclone) supplemented with 10% FBS, 1% penicillin, and streptomycin (10,000 U/mL). To produce cells that stably expressed GFP or RFP, lentiviral GFP and RFP vectors were transduced into 4T1 cells, and 100 μg/mL of G418 was added every other day for 4 weeks to selectively kill the cells without GFP or RFP expression. The colonies were isolated and cultured for another 2 weeks to preserve those cells with a homogeneous genetic background. Paclitaxel and urokinase were purchased from Sigma-Aldrich.

Animal experiments and optical imaging
All of the animal experiments were performed in compliance with institutional guidelines and were approved by the subcommittee on research-animal care at Wonkwang University, South Korea. Both flanks of each mouse were injected with 5×10^5 cells of pure GFP4T1 and RFP4T1 cell lines or mixtures of GFP4T1 and RFP4T1 cell lines. The mice were anesthetized with an intraperitoneal injection of ketamine (90 mg per kg of body weight) and

xylazine (9 mg per kg of body weight) before imaging. Scissors were used to make small incisions around the tumors. The mice were placed on the heated plate of a motorized XYZ translational stage. For vasculature imaging, tetramethylrhodamine (TAMRA) dextran conjugates (5 μg/μL, 2,000,000 MW; Invitrogen) were injected intravenously; the images were typically acquired within 5 to 40 minutes after the injection. GFP-expressing cells were visualized at an excitation wavelength of 491 nm and detected through a bandpass filter of 502 nm to 537 nm (Semrock). TAMRA- and RFP-expressing cells were imaged at an excitation wavelength of 532 nm and detected using a bandpass filter of 562 nm to 596 nm (Semrock).

Urokinase was treated three times a week at 100 U in 100 μL for 4 to 5 weeks.
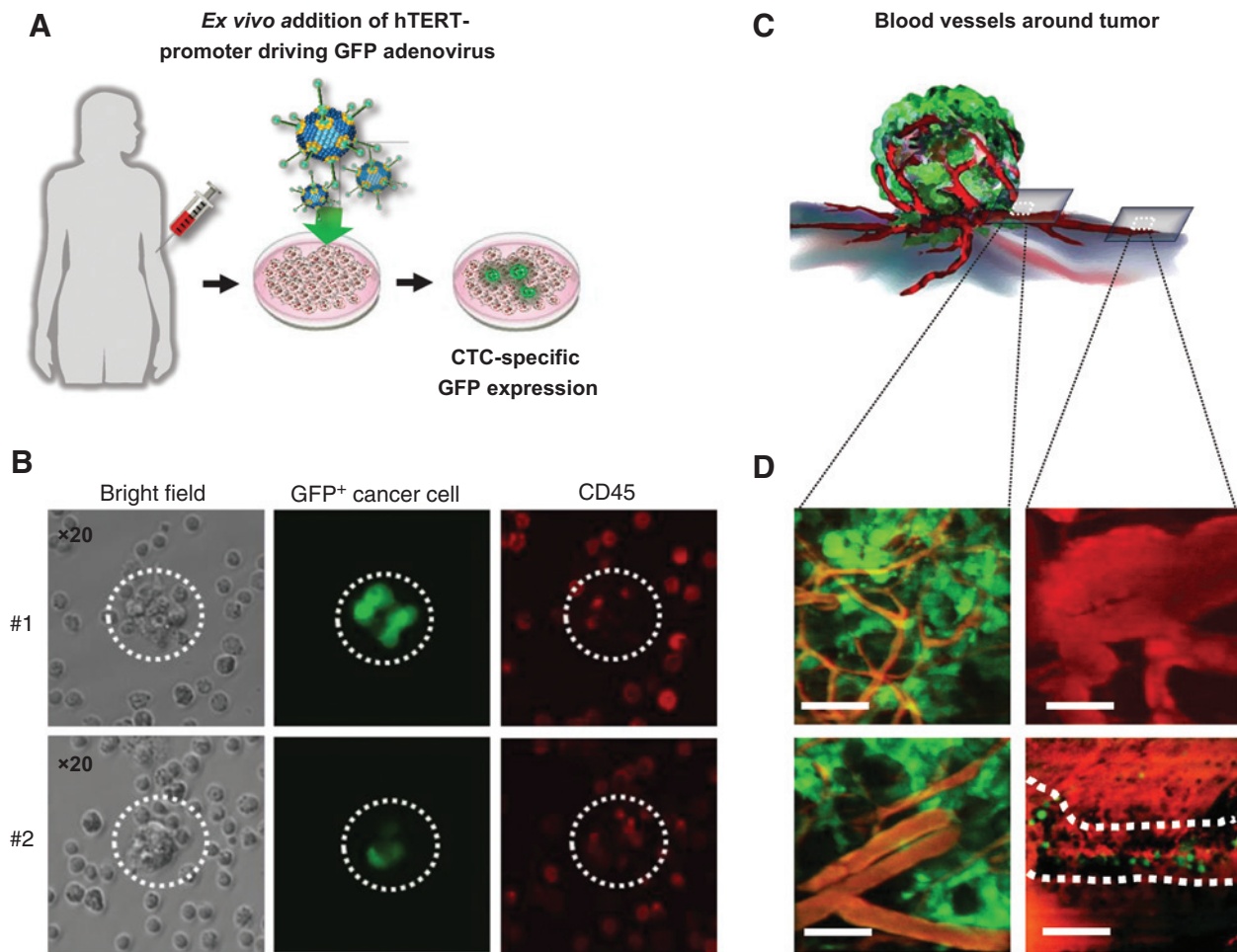
CTC isolation from blood
After the mice were anesthetized, a cardiac puncture was performed. Between 500 μL and 700 μL of the whole blood was collected. After centrifugation, the pellet was incubated with the RBC lysis buffer. The solution containing CTCs was filtered through a strainer of 40 μm mesh size (Corning Life). The cells that remained on the strainer were resuspended in 500 μL of the RPMI culture medium, whereas the rest of the fraction that flowed through the strainer was gently centrifuged again and resuspended in 1 mL of the RPMI. The GFP- and RFP-expressing cells were counted using fluorescence and bright-field microscopy.

Results

Visualization of CTCs in peritumoral regions
Blood samples from patients with breast cancer were used to confirm the existence of a CTC cluster and the heterogeneity of cells in the cluster. To detect CTC with a high specificity and sensitivity, we administrated hTERT-promoter-coding adenoviral vector into blood samples (20–23). GFP was specifically expressed in the CTCs (Fig. 1A and Supplementary Fig. S1). Also, the coexistence of CD45-positive cells—presumably acting as hematopoietic cells—in the CTC clusters was confirmed (Fig. 2B).

To visualize CTCs in blood vessels and evaluate the meaning of the number of CTCs in peritumoral regions, GFP-expressing B16 and B16F10 cells were injected into both flanks of each of the test mice; the latter line is a more metastatic subline derived from B16. The injected cells gradually led to the emergence of visible tumors. At the 5-week mark following the inoculation of the tumor cells, we used intravital, confocal fluorescence microscopy to look at the peritumoral vessels after first making small incisions in the tumor area (Fig. 1C and D). As it is well known that the number of CTCs correlates to the severity of the disease, we compared the number of CTCs from GFP-expressing B16 and B16F10 cells in similar vessels (50–100 μm in diameter) to verify whether the number of CTCs in the peritumoral regions can also be as clinically meaningful as their number in circulation; there were comparatively more B16F10 CTCs than B16 CTCs in such regions (Supplementary Fig. S2A, left, and B). Furthermore, we sought to determine whether treatment with an anticancer drug can affect the number of CTCs. The application of paclitaxel, which had previously been effective for melanomas (24, 25), twice a week for 2 weeks led to a significant decrease in the number of CTCs (Fig. S2A, right, and B). These observations confirmed that, similar to the number of CTCs in circulation, the number of peritumoral CTCs seemed to accurately reflect the metastatic potential of primary tumors.

A *Ex vivo* addition of hTERT-promoter driving GFP adenovirus

CTC-specific GFP expression

B
Bright field | GFP⁺ cancer cell | CD45
#1 ×20
#2 ×20

C Blood vessels around tumor

D

Figure 1.
Validation of CTCs observed in peritumoral regions. A, the scheme to briefly explain the experimental procedure with CTC-specific, hTERT-expressing adenovirus. B, the dotted circles mark the CTC cluster. GFP was expressed at the cluster. CD45 was marked with TRITC to show the hematopoietic cells. C and D, after the incision of skin around the tumor-embedded area, the objective lens was focused on the tumor. Rhodamine-dextran–perfused vessels are visualized in red. Green, tumor tissue containing GFP-expressing B16F10 cells. Scale bar, 50 μm (left); 200 μm (right).

In vivo monitoring of CTC clusters

Interestingly, we occasionally observed clustered cells in peripheral vessels and the numerous GFP-negative cells seemed to be mingled within the CTC cluster (Fig. 1B). To assess the number of CTCs in clusters as a fraction of the total CTC count, movie records were used to count the cells on a weekly basis (Fig. 2A). Although the number of CTCs fluctuated every week, the average CTC count gradually increased as the tumors grew in size during the 5 weeks after the injection of the B16 and B16F10 cells ($n = 5$). The number of CTCs found in clusters also increased; however, they were consistently 5- to 10-fold less abundant than the single CTCs (Fig. 2B).

To confirm the number of CTCs that was counted with live confocal imaging in the peritumoral regions, we compared this number with the number of CTCs obtained from the whole blood. Red fluorescent protein (RFP)-expressing 4T1 cells were used for this purpose and the previously described method was again used. To distinguish the number of cluster CTCs from the total CTC count, we filtered 500 μL of blood with a strainer after the lysis of the red blood cells (RBCs; Fig. 2C). Most of the single cells, including the blood cells and individual CTCs, flowed through the filter and remained in the throttle bottle (Fig. 2C). The CTC clusters were predominantly contained and, to a lesser extent, some CTCs and immune cells were also caught on the strainer sieves (Fig. 2D, top). As the CTCs expressed RFP and their size was somewhat larger than those of other peripheral blood monocyte cells (PBMCs), they were easily distinguished from other cells. As a result, the number of CTCs increased in correspondence with the tumor size and the CTC clusters were much less numerous compared with the single CTCs. We found that the ratio between the clusters and single CTCs was in the range of 1/5 to 1/10; that is, similar to that observed in the *in vivo* confocal microscopy experiments (Fig. 2E). Considering the data illustrated in Fig. 2, we concluded that the number of CTC clusters detected in the peritumoral region was small but was nonetheless meaningfully correlated to the number of CTC clusters in circulation.

Characterization of CTC cluster viscosity and assembly

When the CTC clusters were monitored in real time in a 250-μm width area, they flowed more slowly than the single CTCs, and
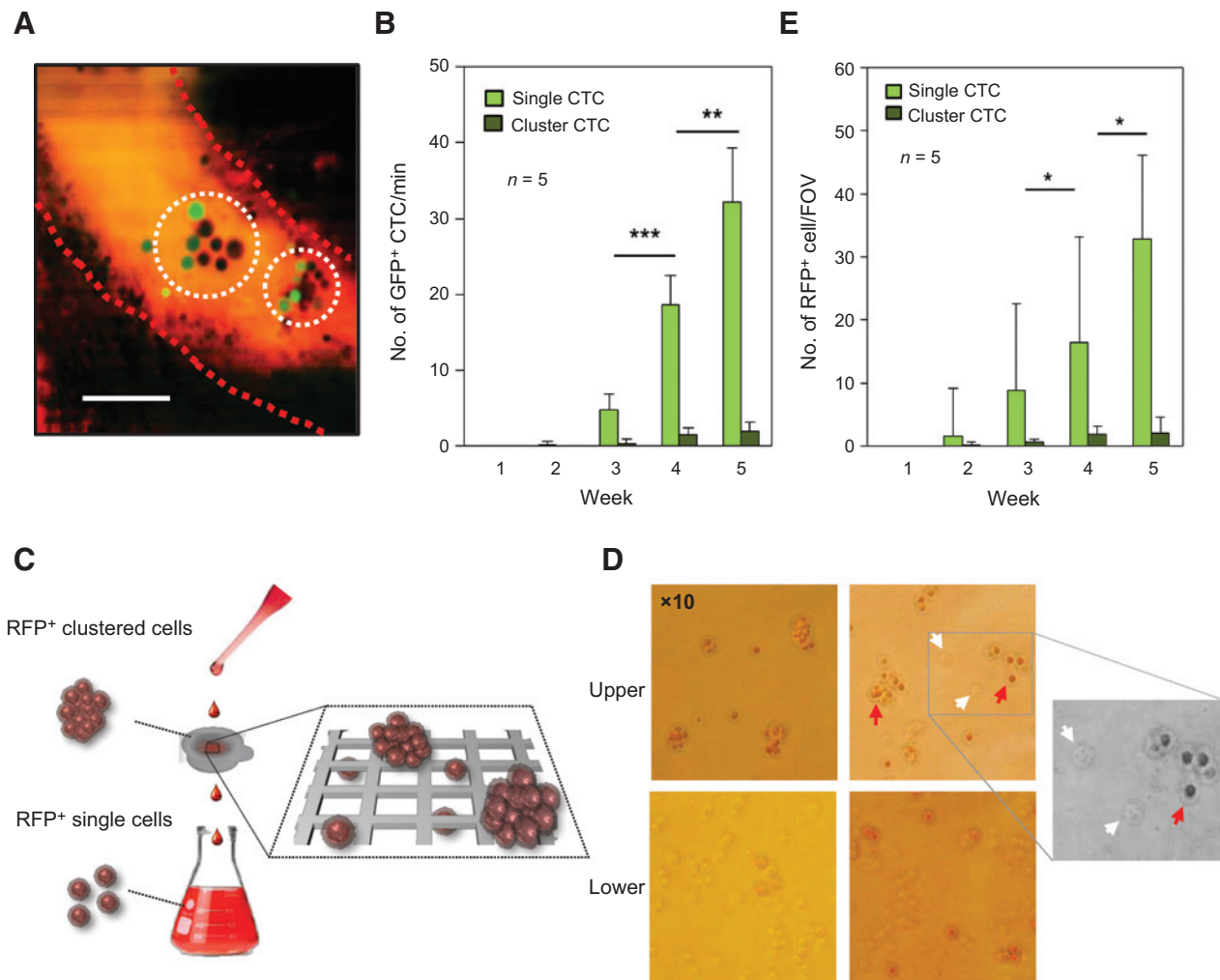
Figure 2.
Increase in the number of CTC clusters with the growth of a tumor. A, a representative image of a CTC cluster. Scale bar, 100 μm. B, the numbers of single CTCs and cluster CTCs that were seen per minute were counted according to progression of cancer. C, whole blood taken by a cardiac puncture was strained to collect and count CTC clusters. Blood flowed through the strainer and the cells that remained on top of the strainer were counted after a resuspension in the culture medium. D, representative panels for RFP-expressing single CTCs that passed through the strainer and CTC clusters that remained on the strainer. The red arrow indicates an RFP-expressing cell, whereas the white arrows point to RFP-negative cells. Scale bar, 200 μm. E, CTCs were counted per single field of view (FOV). The number of CTCs was counted and statistically analyzed from the four randomly taken scopes. $*$, $P < 0.05$; $**$, $P < 0.01$; $***$, $P < 0.001$.

some of them seemed almost static on the vessel surface around the tumors. We sought to make an accurate comparison of the flow-velocity values using both the single and clustered CTCs and found that the average flow speed of the single CTCs was approximately 380 μm/s, which is a little slower than the flow of the GFP-negative PBMCs (~420 μm/second); the flow rate of the CTC clusters was approximately 50 μm/second (Fig. 3A and B). The similar pattern was observed in an orthotopic animal model with mammary fat pad (Fig. 3C and Supplementary Movie S1). The flow rate of the CTC cluster seems to be 10 times slower than single CTCs (Fig. 3D). The clusters slowly rolled within the vessel lumen while the flowing single CTCs became attached to the CTC clusters that were previously formed (Fig. 3E). Therefore, in a case wherein CTC clusters exhibit a comparatively slow speed, their adhesiveness and attachment to vessel walls may be the cause; occasionally, we also observed the GFP-positive tumor cells detach from

the clusters. As we have shown in continuously recorded frames (Fig. 3E and Supplementary Movie S2), the CTC clusters exhibited dynamic compositional changes, as individual CTCs could repeatedly associate with and dissociate from the clusters (Fig. 3E).

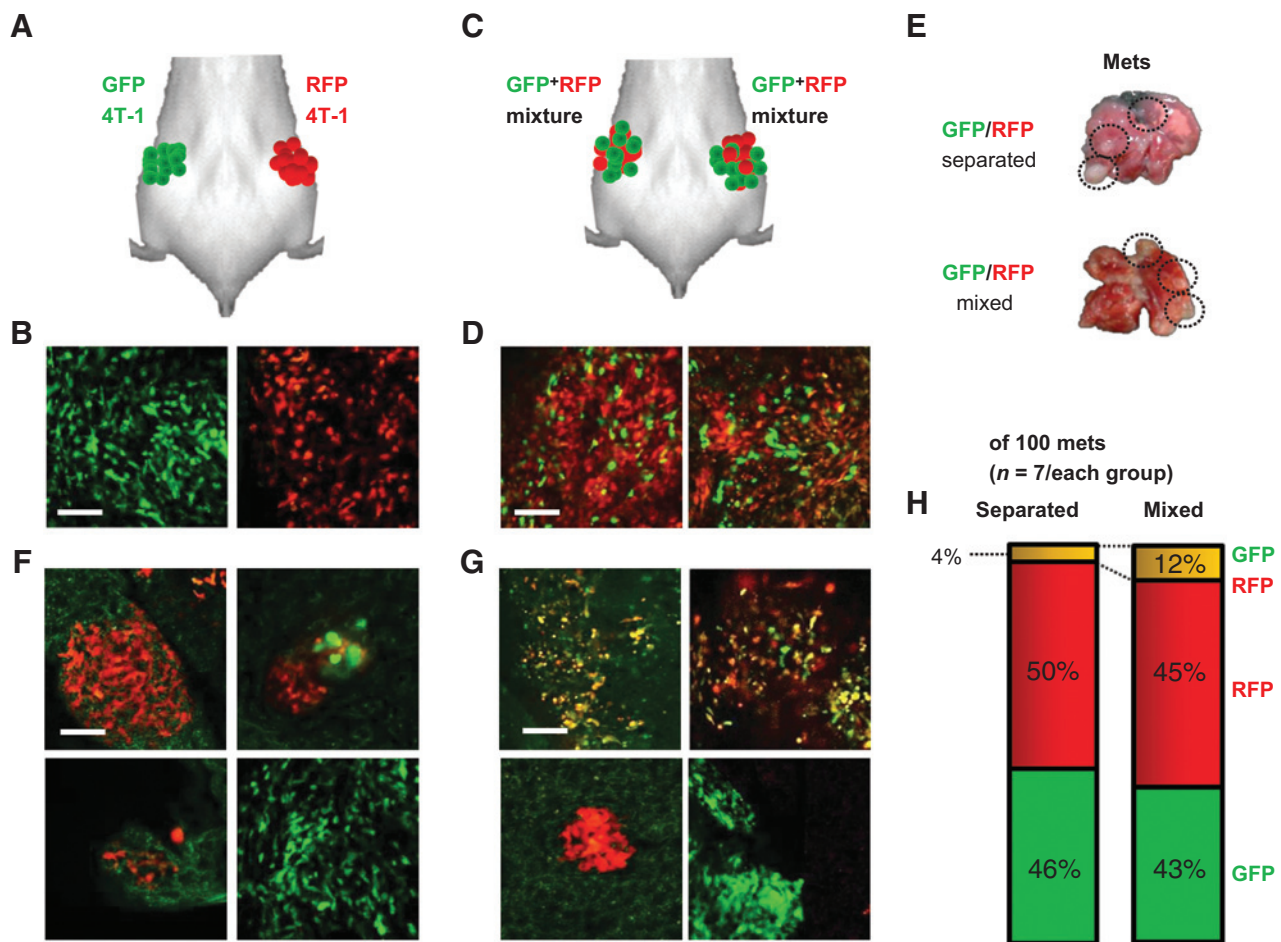### High metastatic potential of CTCs

To assess differences in the abilities of the single CTCs and CTC clusters to metastasize into secondary organs, their metastatic capacities to invade lung tissue were analyzed in an animal model. First, we selected GFP- and RFP-4T1 cells with similar tumorigenic and metastatic activities (Supplementary Fig. S3). In one experimental group, the GFP- and RFP-4T1 cells were separately injected into the opposite flanks of each of the test mice (Fig. 4A and B). In another group, mixtures of GFP-4T1 and RFP-4T1 cells were injected into both flanks, with each side receiving approximately the same number of cells (Fig. 4C and
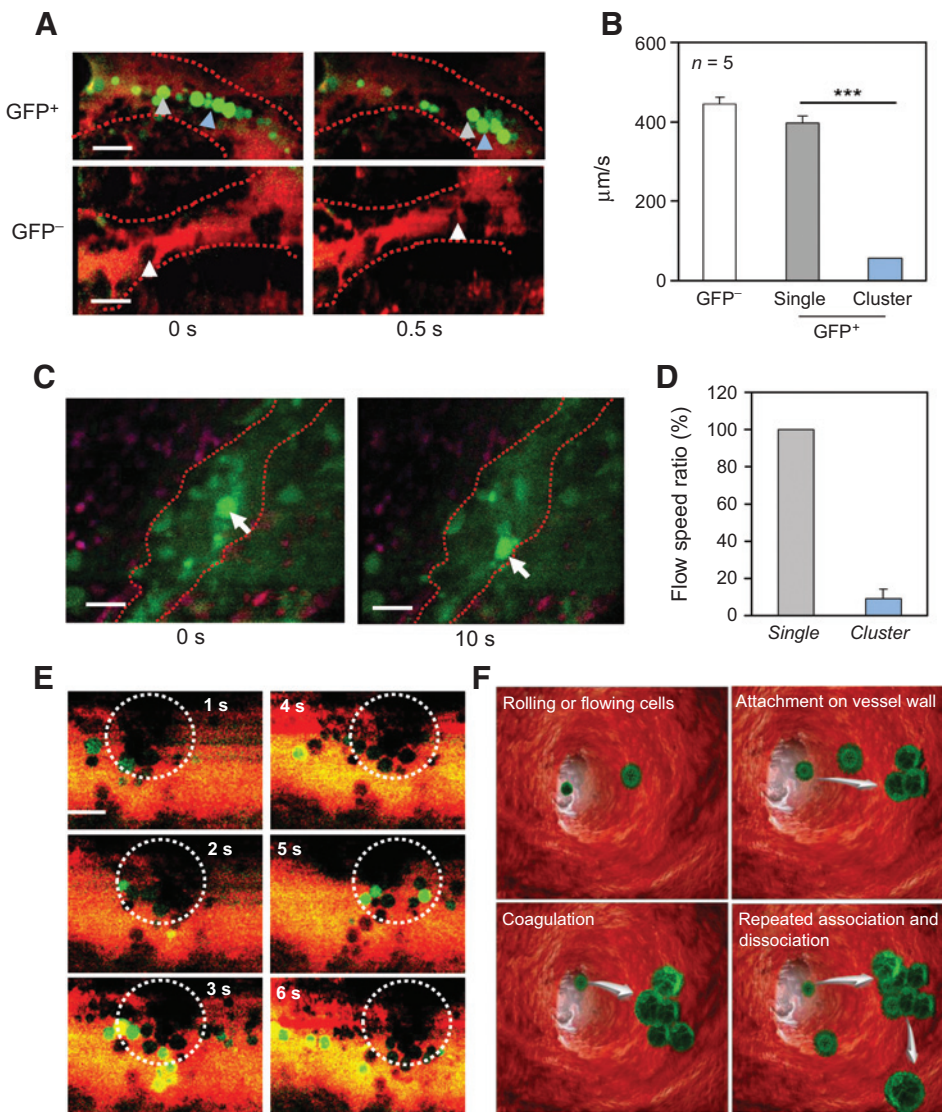
Figure 3.
Real-time imaging-based characterization of CTC clustering. A, the flow rate of the CTC clusters was measured. Top, blue and gray arrows mark a CTC cluster and a single CTC, respectively. Bottom, white arrow, a GFP-negative cell. The flow rate of such cells was taken as a control. Scale bar, 100 μm. B, the flow rate was evaluated and compared between single CTCs, clustered CTCs, and GFP-negative cells. ***, $P < 0.001$. C, slower flow of the CTC cluster was monitored around GFP-4T1 cell–transplanted mammary fat pad for 10 seconds. Scale bar, 100 μm. D, the flow rate of the CTC cluster was compared with the neighbor single CTCs. E, CTC cluster formation was followed by the capturing of a separate image at a rate of 1 Hz for 6 seconds. Scale bar, 100 μm. F, model of the CTC-cluster-formation process is illustrated based on the observed dynamics.

D). Five weeks after the inoculation, the mice's lungs were dissected and analyzed (Fig. 4E). We found comparable numbers of metastasized nodules in the experimental groups, implying the similar metastatic potentials of GFP- and RFP-4T1 cells (Fig. 4E). The nodules from each group were examined using a confocal microscope to observe the composition of the metastasized cells. We dissected 100 nodules from 7 mice in each group. Eleven to 16 nodules from each mouse were randomly selected based on the nodule size. When we observed each nodule under a confocal microscope, the nodules could be divided into the following three groups according to their fluorescent colors: nodules expressing exclusively GFP or RFP, and nodules simultaneously expressing both fluorescent proteins. The number of nodules in each category was counted and the totals were compared between the experimental groups (Supplementary Table S1). In the mice that received separate injections of GFP- and RFP-tagged cells, 46% of the nodules expressed only GFP and another 50% expressed only RFP; the remaining 4% of nodules contained a mixture of GFP and RFP

colors (Fig. 4G and H, left bar). In the mice that were injected with mixtures of GFP- and RFP-tagged cells, the fractions of single-color nodules were slightly decreased compared with the mice that received separate injections of pure-cell populations. In the mixture-injected mice, the GFP- and RFP-containing nodules were measured at 43% and 45%, respectively. Consequently, the fraction of nodules containing both GFP- and RFP-positive cells increased to 12% (Fig. 4H). A difference of 8% in the fraction of nodules with mixed GFP- and RFP-positive cells was therefore identified between the first and second experimental groups. It is likely that every nodule of a uniform color was derived from a single site that the CTCs initially infiltrated; although, according to our observations, 8% of the nodules potentially originated from the mixed CTC clusters. Furthermore, even in those nodules that expressed only GFP or RFP, the same 8% probability regarding the coexistence of same-colored cells from different clusters could be expected, as previously mentioned. The nodules that emerged from the CTC clusters may therefore account for as much as 24% (= 3 × 8%) of all of

Figure 4.
Comparison of the metastatic potential of single and cluster CTCs. A and B, GFP-4T1 and RFP-4T1 cells were respectively inoculated into the left and right flanks of a mouse. A confocal microscope was used to visualize the primary tumor. Scale bar, 100 μm. C and D, mixtures of GFP-4T1 and RFP-4T1 cells were separately injected into both flanks. The primary tumor was visualized. Scale bar, 100 μm. E, five weeks after the cell inoculation, the lung tissue was isolated. Dotted circles mark metastasized nodules. F, representative nodules visualized by confocal microscopy in the lungs of animals injected with either GFP- or RFP-expressing cells. Scale bar, 100 μm. G, representative nodules in the lungs of animals injected with mixtures of GFP and RFP cells. Scale bar, 100 μm. H, distribution of nodules containing only GFP-labeled cells (green), RFP-labeled cells (red), or a mixture of both (yellow). The lengths of the colored bars reflect the fractions of the corresponding cell populations.

the nodules that were observed. Our finding, whereby the GFP- and RFP-mixed nodules occurred more frequently in those animals that were injected with mixtures of GFP- and RFP-positive cells, indicates that clusters mainly form around primary tumors and not during circulation.
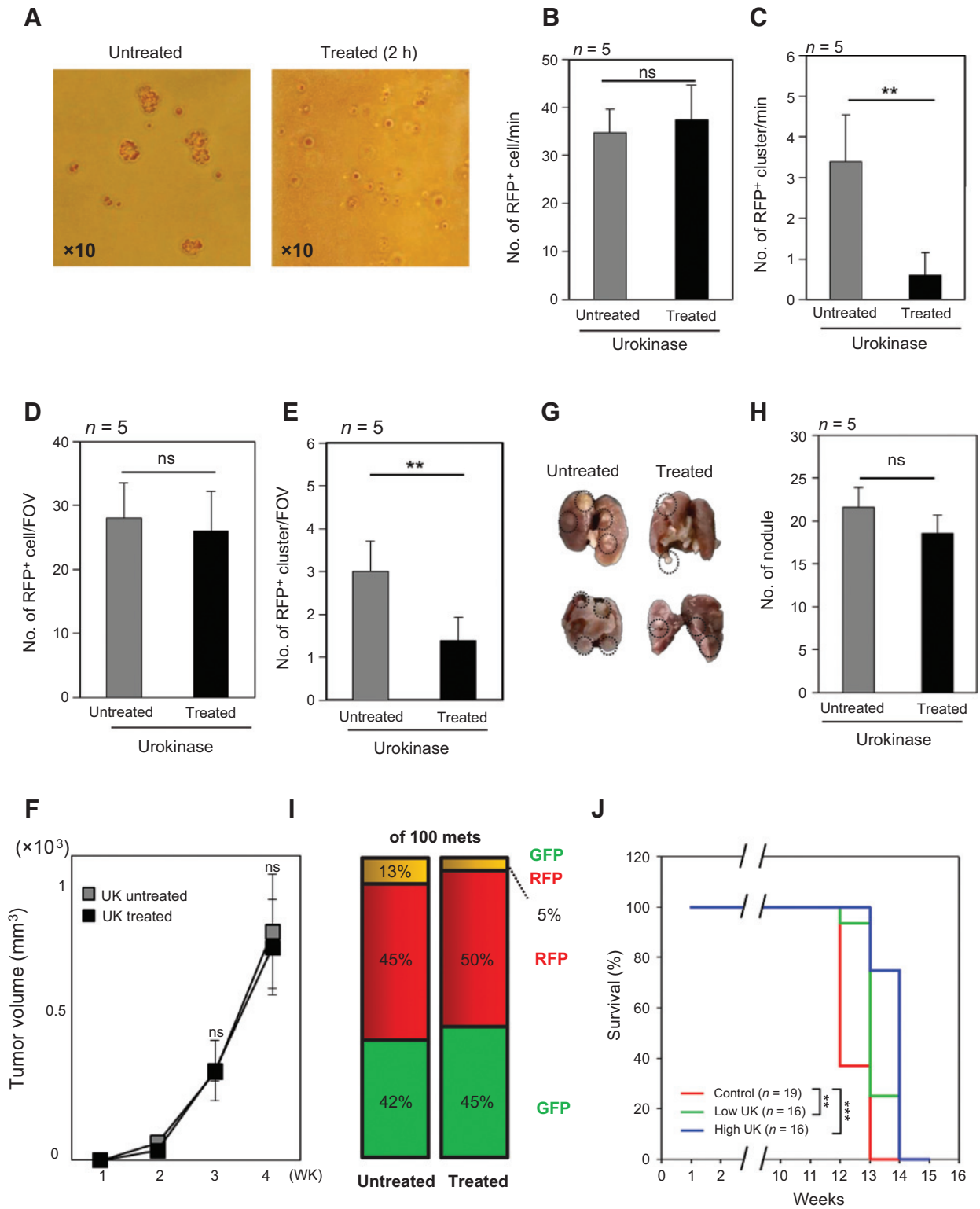
Effect of urokinase on CTC clusters

Fibrin is considered to be an inducer of CTC clustering (26, 27); therefore, we sought to determine whether urokinase, a thrombolytic agent that dissolves fibrin, suppresses the clustering of CTCs *in vitro* and affects metastasis *in vivo*. We observed a reduction in the number of CTC clusters on the sieves after an *in vitro* incubation with 0.2 mg/mL urokinase for 10 minutes (Fig. 5A). *In vivo* treatment with 100 U of urokinase decreased the number of CTC clusters in the blood of treated mice compared with the numbers in the control, untreated animals, whereas the number of single CTCs was not affected (Fig. 5B and C); *in vivo* confocal-microscopy–based observations of the areas around the tumors

showed the reproduction of this pattern (Fig. 5E and F). Collectively, these results suggest that urokinase directly breaks down CTC clusters into single CTCs.

To confirm the inhibitory effect of urokinase on CTC clustering *in vivo*, cell mixtures containing 50% GFP-positive and 50% RFP-positive 4T1 cells were injected into both flanks of each of the mice, as described in the experiments that are depicted in Fig. 4C, followed by the administration of urokinase once or twice a week for 3 weeks after the inoculation. The treatment with urokinase did not affect the growth of primary tumors (Fig. 5F); however, the thrombolytic agent seemed to reduce metastasis (Fig. 5H). We used confocal microscopy to analyze the color composition of the metastasized nodules. Each nodule was again assigned to one of the three groups based on the fluorescent colors that it expressed. Interestingly, the population of nodules that comprised both GFP- and RFP-tagged cells decreased from 13% to 5% after the urokinase treatment (Fig. 5I). The change of this proportion was statistically significant

Figure 5.
Antimetastatic and anticlustering effects of urokinase on CTCs. A, the number of CTC clusters was compared before and after the incubation of the CTCs with urokinase *in vitro.* Representative images before (left) and after (right) urokinase treatment. B, the number of single CTCs after urokinase treatment was counted under a confocal microscope. C, the number of CTC clusters was counted using the above method. The numbers of single CTCs (D) and CTC clusters (E) were counted after filtering with a strainer, before and after urokinase treatment. ns, not significant; **, $P < 0.01$. FOV, field of view. F, following urokinase treatment, the growth rate of the primary tumors was measured every week until the fourth week after the tumor-cell inoculation. G, representative photos of lungs with metastases isolated from urokinase-treated and untreated groups are presented. H, the numbers of nodules were counted and plotted on a bar graph. I, upon urokinase treatment, only the fractions of nodules containing GFP-labeled cells (green), RFP-labeled cells (red), or a mixture of both (yellow) were calculated. The lengths of the colored bars reflect the fractions of the corresponding cell populations. J, evaluation of the survival of the mice injected with the vehicle (control) or urokinase (low and high dose). Statistics was calculated by the log-rank test. **, $P < 0.01$; ***; $P < 0.001$

($P = 0.035$) in accordance with the Fisher exact test; also, the ratio between the nodules that exclusively expressed RFP or GFP was preserved (Fig. 5I). Finally, to determine whether urokinase can improve the survival of animals implanted with cancer cells, we administered the mice with urokinase once or twice a week for 3 weeks after the cell inoculation. The total survival periods of the mice that were treated weekly were prolonged on average by 5 to 6 days in low-dose and by 9 to 10 days in high-dose group, thus the total survival periods of those urokinase-treated mice were improved more significantly ($P < 0.01$) in comparison with the untreated animal group. As the tumor cells were implanted Week 7 and the death was initiated from Week 12, it means the survival extension is more than 20% considering the diagnosed time point and life span.

Discussion

Metastasis has fatal consequences for patients with cancer, while CTCs are considered the "seeds" of metastasis. To spread to distant organs, cancer cells need to enter the blood vasculature and become CTCs; this process is considered a critical step in the metastatic process. Furthermore, the flow of CTCs in the bloodstream is the last step before they disseminate into a secondary organ (1–3). Once metastasized, cancer becomes more difficult to treat, so the detection of CTCs can predict clinical output, and may be used in the monitoring of the efficacy of pharmacologic interventions against metastases. In addition, a number of CTCs can form a clump, also referred to as a "cluster" in this manuscript. According to a general understanding, CTC clusters are directly responsible for metastases, as they exhibit a higher metastatic property than individual CTCs. Many tumor cells possess strong pro-coagulant properties that promote the local activation of the coagulation system (28–30). Tumor-mediated stimulation of coagulation has been implicated in the formation of tumor stroma and the development of hematogenous metastasis (30–34).

As illustrated in Fig. 2, we observed the adherence of CTC clusters to blood vessels. It was most likely that the clusters that appeared to contain GFP-negative cells as well as GFP-positive cells were composed of CTCs. Although platelets can be one of the components of CTC clusters, it is plausible that the GFP-negative cells that we observed were actually macrophages rather than platelets, as their diameter was 10 to 20 μm (35), whereas a platelet's diameter is normally under 2 μm (36, 37). Tumor-associated macrophages induce the formation of CTC clusters around blood vessels near the tumor, establishing gradients of the EGF within the tumor environment; this process can also lead to the attraction of tumor cells toward blood vessels (38, 39).

Fibrinogen is likely to play an important role in the emergence of CTC clumps. The majority of solid tumors in humans and experimental animals contain considerable amounts of fibrinogen-related products—mostly cross-linked fibrin—suggesting that fibrin and fibrinogen are important in tumorigenesis and metastasis (40–44). Research has found that fibronectin has also been upregulated in several types of malignant tumors, and its expression positively correlates to an invasive and metastatic phenotype. Low-molecular weight (LMW) heparin directly leads to fibrin lysis, and patients treated with LMW heparin have a significant survival benefit; however, research has still not conclusively verified if the antimetastatic effect of heparins and other antithrombotic agents is clinically beneficial (45, 46). The ability of thrombolytics such as urokinase to break cell aggregates is well documented and this property is sometimes used to treat intravascular coagulation in cancer patients (47). The pharmacologic mechanism-of-action of this drug targets cell-aggregation–promoting fibrin. To decrease the number of CTC clusters, urokinase, which can break down blood clots, was intravenously injected into those mice that had previously developed lung cancer (Fig. 5), and the injections successfully increased the survival rate of those mice with lung cancer metastases; therefore, our findings demonstrate an ample therapeutic potential of the manipulations of CTC clusters that could minimize cancer metastases. Moreover, our data suggest that the antimetastatic effect of coagulation inhibition may partially come from the disassembling of CTC clusters. In a previous study, plakoglobin seemed to be a promising therapeutic drug for inhibiting the formation of CTC clusters (5). As the antimetastatic effect of siRNA against plakoglobin caused an inhibition of cell aggregation in circulation, the direct manipulation of fibrinogen may be another promising method to control CTC clusters, in addition to the targeting of plakoglobin.

Improvements in optical-imaging techniques have now enabled us to obtain far more precise observations of metastasizing cells, and confocal imaging of tumors that express fluorescent proteins enables researchers to conduct detailed observations of cell motility. Although it is not easy to observe a CTC cluster in circulation with a microscope, our intravital imaging reliably detected CTC clusters that emerged near primary tumors. The development of the CTC clusters in the peritumoral region was confirmed by an analysis of the results obtained from those cells expressing GFP, RFP, or a mixture of both fluorescent proteins (Fig. 4). Our calculations showed results that are comparable with those obtained by Aceto and colleagues in radiolabeled cells.

Therefore, while the previous studies on CTCs relied on the isolation of such cells from the blood, our imaging-based observations helped us to directly understand the dynamics of CTCs and the clustering process in blood vessels. This analysis on the CTC cluster with the patients may give a benefit to predict disease progression. And the trial with *in vivo* or *ex vivo* screening system that looks for an active intervention into CTC cluster formation may lead a novel drug discovery for the treatment of cancer before it starts disseminating into the secondary organs.

References

1. Chaffer CL, Weinberg RA. A perspective on cancer cell metastasis. Science 2011;331:1559–64.
2. de Wit S, van Dalum G, Terstappen LW. Detection of circulating tumor cells. Scientifica 2014;2014:819362.
3. Gupta GP, Massague J. Cancer metastasis: building a framework. Cell 2006;127:679–95.
4. Molnar B, Ladanyi A, Tanko L, Sreter L, Tulassay Z. Circulating tumor cell clusters in the peripheral blood of colorectal cancer patients. Clin Cancer Res 2001;7:4080–5.
5. Aceto N, Bardia A, Miyamoto DT, Donaldson MC, Wittner BS, Spencer JA, et al. Circulating tumor cell clusters are oligoclonal precursors of breast cancer metastasis. Cell 2014;158:1110–22.
6. Fidler IJ. The relationship of embolic homogeneity, number, size and viability to the incidence of experimental metastasis. Eur J Cancer 1973; 9:223–7.
7. Liotta LA, Saidel MG, Kleinerman J. The significance of hematogenous tumor cell clumps in the metastatic process. Cancer Res 1976;36:889–94.
8. Glaves D. Correlation between circulating cancer cells and incidence of metastases. Br J Cancer 1983;48:665–73.
9. Gao Y, Yuan Z. Nanotechnology for the detection and kill of circulating tumor cells. Nanoscale Res Lett 2014;9:500.
10. Nagrath S, Sequist LV, Maheswaran S, Bell DW, Irimia D, Ulkus L, et al. Isolation of rare circulating tumour cells in cancer patients by microchip technology. Nature 2007;450:1235–9.
11. Joosse SA, Gorges TM, Pantel K. Biology, detection, and clinical implications of circulating tumor cells. EMBO Mol Med 2014;7:1–11.
12. Riethdorf S, Fritsche H, Muller V, Rau T, Schindlbeck C, Rack B, et al. Detection of circulating tumor cells in peripheral blood of patients with metastatic breast cancer: a validation study of the CellSearch system. Clin Cancer Res 2007;13:920–8.
13. Ozkumur E, Shah AM, Ciciliano JC, Emmink BL, Miyamoto DT, Brachtel E, et al. Inertial focusing for tumor antigen-dependent and -independent sorting of rare circulating tumor cells. Sci Transl Med 2013;5:179ra47.
14. Stott SL, Hsu CH, Tsukrov DI, Yu M, Miyamoto DT, Waltman BA, et al. Isolation of circulating tumor cells using a microvortex-generating herringbone-chip. Proc Natl Acad Sci U S A 2010;107:18392–7.
15. Condeelis J, Segall JE. Intravital imaging of cell movement in tumours. Nat Rev Cancer 2003;3:921–30.
16. Wessels JT, Busse AC, Mahrt J, Dullin C, Grabbe E, Mueller GA. *In vivo* imaging in experimental preclinical tumor research–a review. Cytometry A 2007;71:542–9.
17. Sahai E. Illuminating the metastatic process. Nat Rev Cancer 2007;7: 737–49.
18. Emptage NJ. Fluorescent imaging in living systems. Curr Opin Pharmacol 2001;1:521–5.
19. Stemmer A, Beck M, Fiolka R. Widefield fluorescence microscopy with extended resolution. Histochem Cell Biol 2008;130:807–17.
20. Gorges TM, Tinhofer I, Drosch M, Rose L, Zollner TM, Krahn T, et al. Circulating tumour cells escape from EpCAM-based detection due to epithelial-to-mesenchymal transition. BMC Cancer 2012;12:178.
21. Kishimoto H, Kojima T, Watanabe Y, Kagawa S, Fujiwara T, Uno F, et al. *In vivo* imaging of lymph node metastasis with telomerase-specific replication-selective adenovirus. Nat Med 2006;12:1213–9.
22. Kojima T, Hashimoto Y, Watanabe Y, Kagawa S, Uno F, Kuroda S, et al. A simple biological imaging system for detecting viable human circulating tumor cells. J Clin Invest 2009;119:3172–81.
23. Shigeyasu K, Tazawa H, Hashimoto Y, Mori Y, Nishizaki M, Kishimoto H, et al. Fluorescence virus-guided capturing system of human colorectal circulating tumour cells for non-invasive companion diagnostics. Gut 2015;64:627–35.
24. Einzig AI, Hochster H, Wiernik PH, Trump DL, Dutcher JP, Garowski E, et al. A phase II study of taxol in patients with malignant melanoma. Invest New Drugs 1991;9:59–64.
25. Einzig AI, Wiernik PH, Schwartz EL. Taxol: a new agent active in melanoma and ovarian cancer. Cancer Treat Res 1991;58:89–100.
26. Im JH, Fu W, Wang H, Bhatia SK, Hammer DA, Kowalska MA, et al. Coagulation facilitates tumor cell spreading in the pulmonary vasculature during early metastatic colony formation. Cancer Res 2004;64:8613–9.
27. Karpatkin S, Pearlstein E. Role of platelets in tumor cell metastases. Ann Intern Med 1981;95:636–41.
28. Donati MB. Cancer and thrombosis: from Phlegmasia alba dolens to transgenic mice. Thromb Haemost 1995;74:278–81.
29. Dvorak HF. Thrombosis and cancer. Hum Pathol 1987;18:275–84.
30. Dvorak HF, Nagy JA, Berse B, Brown LF, Yeo KT, Yeo TK, et al. Vascular permeability factor, fibrin, and the pathogenesis of tumor stroma formation. Ann N Y Acad Sci 1992;667:101–11.
31. Cavanaugh PG, Sloane BF, Honn KV. Role of the coagulation system in tumor-cell-induced platelet aggregation and metastasis. Haemostasis 1988;18:37–46.
32. Esumi N, Fan D, Fidler IJ. Inhibition of murine melanoma experimental metastasis by recombinant desulfatohirudin, a highly specific thrombin inhibitor. Cancer Res 1991;51:4549–56.
33. Mueller BM, Ruf W. Requirement for binding of catalytically active factor VIIa in tissue factor-dependent experimental metastasis. J Clin Invest 1998;101:1372–8.
34. Walz DA, Fenton JW. The role of thrombin in tumor cell metastasis. Invasion Metastasis 1994;14:303–8.
35. Krombach F, Munzing S, Allmeling AM, Gerlach JT, Behr J, Dorger M. Cell size of alveolar macrophages: an interspecies comparison. Environ Health Perspect 1997;105 Suppl 5:1261–3.
36. Paulus JM. Platelet size in man. Blood 1975;46:321–36.
37. Slack SM, Jennings LK, Turitto VT. Platelet size distribution measurements as indicators of shear stress-induced platelet aggregation. Ann Biomed Eng 1994;22:653–9.
38. Smith HA, Kang Y. The metastasis-promoting roles of tumor-associated immune cells. J Mol Med 2013;91:411–29.
39. Wang W, Goswami S, Sahai E, Wyckoff JB, Segall JE, Condeelis JS. Tumor cells caught in the act of invading: their strategy for enhanced cell motility. Trends Cell Biol 2005;15:138–45.
40. Bardos H, Molnar P, Csecsei G, Adany R. Fibrin deposition in primary and metastatic human brain tumours. Blood Coagul Fibrinolysis 1996;7: 536–48.
41. Brown LF, Van de Water L, Harvey VS, Dvorak HF. Fibrinogen influx and accumulation of cross-linked fibrin in healing wounds and in tumor stroma. Am J Pathol 1988;130:455–65.
42. Dvorak HF. Tumors: wounds that do not heal. Similarities between tumor stroma generation and wound healing. N Engl J Med 1986;315:1650–9.
43. Dvorak HF, Harvey VS, McDonagh J. Quantitation of fibrinogen influx and fibrin deposition and turnover in line 1 and line 10 guinea pig carcinomas. Cancer Res 1984;44:3348–54.
44. Harris NL, Dvorak AM, Smith J, Dvorak HF. Fibrin deposits in Hodgkin's disease. Am J Pathol 1982;108:119–29.
45. Hettiarachchi RJ, Smorenburg SM, Ginsberg J, Levine M, Prins MH, Buller HR. Do heparins do more than just treat thrombosis? The influence of heparins on cancer spread. Thromb Haemost 1999;82:947–52.
46. Zacharski LR, Meehan KR, Algarra SM, Calvo FA. Clinical trials with anticoagulant and antiplatelet therapies. Cancer Metastasis Rev 1992; 11:421–31.
47. Myohanen H, Vaheri A. Regulation and interactions in the activation of cell-associated plasminogen. Cell Mol Life Sci 2004;61:2840–58.

Urokinase Exerts Antimetastatic Effects by Dissociating Clusters of Circulating Tumor Cells

Jin Woo Choi, Jun Ki Kim, Yun Jung Yang, et al.

Updated version	Access the most recent version of this article at: http://cancerres.aacrjournals.org/content/75/21/4474
Supplementary Material	Access the most recent supplemental material at: http://cancerres.aacrjournals.org/content/suppl/2015/11/06/75.21.4474.DC1.html

Cited articles	This article cites 47 articles, 11 of which you can access for free at: http://cancerres.aacrjournals.org/content/75/21/4474.full.html#ref-list-1

E-mail alerts	Sign up to receive free email-alerts related to this article or journal.
Reprints and Subscriptions	To order reprints of this article or to subscribe to the journal, contact the AACR Publications Department at pubs@aacr.org.
Permissions	To request permission to re-use all or part of this article, contact the AACR Publications Department at permissions@aacr.org.